IEEE Access
Multidisciplinary ⋮ Rapid Review ⋮ Open Access Journal

Received 27 October 2023, accepted 10 November 2023, date of publication 16 November 2023,
date of current version 28 November 2023.

Digital Object Identifier 10.1109/ACCESS.2023.3333694

RESEARCH ARTICLE

Cell Alignment in Aqueous Solution Employing a Flexural Plate Wave Piezoelectric MEMS Transducer

ALESSANDRO NASTRO[1], (Member, IEEE), MARCO BAÙ[1], (Member, IEEE), MARCO FERRARI[1], (Member, IEEE), LIBOR RUFER[2], (Senior Member, IEEE), SKANDAR BASROUR[3], (Member, IEEE), AND VITTORIO FERRARI[1], (Senior Member, IEEE)

[1]Department of Information Engineering, University of Brescia, 25123 Brescia, Italy
[2]ADT MEMS, 38140 Rives, France
[3]Univ. Grenoble Alpes, CNRS, Grenoble Institute of Engineering Univ. Grenoble Alpes, TIMA, 38000 Grenoble, France

Corresponding author: Alessandro Nastro (alessandro.nastro@unibs.it)

ABSTRACT The possibility to steer floating cells dispersed in water by means of flexural plate waves (FPWs) generated by a 9 mm × 9 mm piezoelectric MEMS transducer has been explored. The MEMS transducer has a squared cavity etched out in a silicon substrate formed by a 6 mm × 6 mm composite diaphragm made of a piezoelectric aluminum nitride (AlN) layer on top of a doped silicon plate. The piezoelectric layer can be electrically actuated by means of metal interdigital transducers (IDTs) placed over the AlN film at the diaphragm edges. Cell alignment has been sought for by inducing standing FPWs in the diaphragm and in the contacting water layer in the cavity by the one-dimensional (1D) acoustic field pattern obtained by exciting two IDTs located symmetrically with respect to the diaphragm centre. The working principle has been validated by means of 2D finite element modelling and simulations. The MEMS transducer has been fabricated using the PiezoMUMPs process and experimentally tested by exploiting a tailored front-end electronic circuit. Inactive fibroblast cells with an approximate diameter of 15 μm have been dispersed in demineralized water within the cavity at a concentration in the order of 10^5 cells/ml. By applying sinusoidal excitation signals to faced IDTs with zero phase shift and peak amplitude of 10 V, lines of cells spaced by half wavelength $\lambda/2 = 56$ μm have been achieved at 12.5 MHz, in good agreement with theoretical predictions and simulation results.

INDEX TERMS Cell alignment, acoustic waves, flexural plate waves, lamb waves, MEMS, piezoelectric, PiezoMUMPs, transducer, COMSOL multiphysics, FEM, electrical admittance.

I. INTRODUCTION

The alignment of cells plays a crucial role in fundamental biological analyses and medical applications. Advances in tissue engineering have significantly improved cell alignment to restore, analyse, or even replace different types of biological tissues. In biofabrication of blood vessels, the achievement of aligned and functional endothelial cells is of utmost importance as they form the inner lining of all blood vessel walls [1]. The alignment of collagen fibers has been correlated to breast cancer cell invasion and identified as one of the key factors to determine in advance cell abnormalities related to human diseases [2]. Numerous studies have demonstrated that oriented biomaterials can accelerate and promote directional regrowth of damaged axons for brain injuries repair [3], [4]. The field of tissue engineering relies on the development of alignment supports or techniques that can act as templates for tissue formation employable *in vitro*, as guidance for cellular regeneration, or *in vivo*, as founding structures for tissue growth [5]. For *in vivo* cell alignment, hydrodynamic materials [6] or scaffolds are typically employed as structural components. Electrically conductive

The associate editor coordinating the review of this manuscript and approving it for publication was Shuo Sun.

collagen scaffolds for skeletal muscle tissue engineering have been developed to align and differentiate myoblast cells [7]. Whereas, *in vitro* cell alignment approaches are normally based on the exploitation of external stimuli and fields. For instance, optical tweezers rely on forces exerted by a focused beam of light to trap and pattern cells [8], [9]. Magnetic tweezers exploit a magnetic field gradient in which particles are placed and are subjected to forces related to fluid magnetization [10]. Electrokinetic-based approaches use electrosurface phenomena with embedded microelectrodes to pattern cells [11], [12]. In general, the main issue while dealing with alignment supports or techniques is their biocompatibility, i.e., the ability to obtain the desired function without causing any local or systemic adverse response in the cells [13]. To this extent, acoustophoresis has attracted attention to manipulate cells through acoustic waves, due to its intrinsic label-free, non-contact, and non-invasive properties [14]. Acoustophoresis is commonly achieved by inducing in piezoelectric materials acoustic waves due to the applied electrical excitation signals [15]. Acoustic waves are then employed as a coupling mean to exchange energy and to induce forces into the liquid where cells are typically dispersed [16]. Specifically, in a standing wave field the acoustic radiation force (ARF) drives the particles dispersed in liquid into acoustic pressure nodes, thus allowing their manipulation and alignment [17], [18]. Bulk acoustic waves (BAW) [19], surface acoustic waves (SAW) [20], and flexural plate waves (FPW) [21], are typical acoustic modes exploited in piezoelectric transducers. The adoption of FPWs has the advantage of exhibiting a wave velocity that decreases with decreasing plate thickness and may become lower than the wave velocity in liquids. Therefore, for a given wavelength, the corresponding frequency is relatively low, i.e. typically in the range of 5-20 MHz, which alleviates the requirements on the associated driving electronics compared to typical SAW devices. Furthermore, FPW sensors are suitable for the measurement of fluid properties, such as liquid viscosity, and gravimetric (bio)chemical analysis in solutions [22].

In this context, the present work proposes a piezoelectric MEMS transducer able to generate an acoustic field pattern based on standing FPWs for the alignment of cells in aqueous solution. The working principle has been investigated through a 2D finite element modelling and confirmed by comparing the obtained simulations with experimental results. A tailored front-end circuit based on a direct digital synthesizer has been designed to drive the device. With inactive fibroblast cells dispersed in demineralized water placed in the MEMS cavity, the applied excitation signals have allowed to align cells along a regular pattern with a spacing equal to half the acoustic wavelength. The present work extends the early contents reported in the conference paper [23] providing details of the working principle of the MEMS transducer related to the acoustic-fluidic coupling, including a 2D FEM model, adding the comparison of the electrical measurements with the simulation results of the single IDT admittance and describing the tailored front-end electronics employed for cell alignment. The paper is organized as follows: Working principle (Section II), MEMS description (Section III), Finite element analysis (Section IV), Experimental results (Section V) and Conclusions (Section VI).

II. WORKING PRINCIPLE

Top and bottom schematic views of the proposed MEMS transducer are shown in Figure 1a,b, respectively. The device embeds a squared cavity etched out in a silicon substrate and a composite piezoelectric-silicon diaphragm for steering and confining floating cells in liquid. The diaphragm can be electrically actuated by means of metal interdigital transducers (IDTs) deposited on the piezoelectric film. Each IDT is formed by two interleaved comb-shaped electrodes of equally spaced fingers with pitch p larger than the diaphragm thickness. By applying a sinusoidal excitation voltage between the IDT fingers, the converse piezoelectric effect is exploited to induce a dynamic deformation of the piezoelectric layer thickness and of the diaphragm in turn. As a consequence, Lamb waves are generated in the diaphragm which are coupled to the liquid in the cavity. In this work, by applying sinusoidal excitation voltages to two IDTs located symmetrically with respect to the cavity centre, the first antisymmetric vibrational mode (A0) of the diaphragm is exploited to achieve standing flexural plate waves (FPWs) with wavelength λ, as shown in Figure 1c. In turn, compressional acoustic waves are coupled into the liquid generating a one-dimensional (1D) acoustic field pattern in which pressure nodes are located at half the acoustic wavelength $\lambda/2$ [24]. The cells dispersed in the liquid are thus steered and trapped in distinct positions by the developed forces. Specifically, along the vertical y-axis the equilibrium position of each cell is determined by the force balance between gravity and buoyancy [25]. On the other hand, along the horizontal x-axis crossing the IDTs, each cell is subjected to the acoustic radiation force (ARF) and the viscous force [26]. For floating cells with diameter larger than 3 μm the ARF typically exceeds the viscous force and pushes each cell toward the nearest

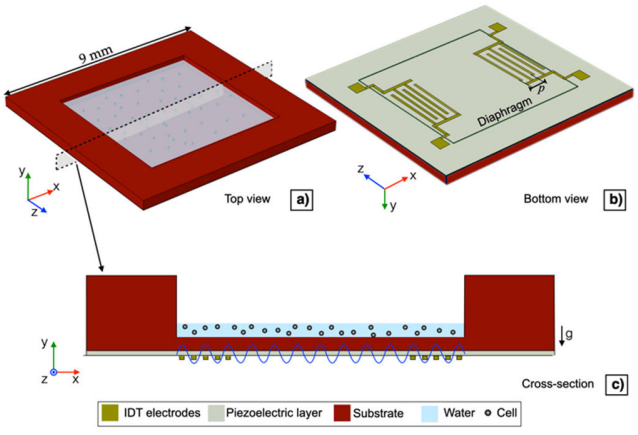

FIGURE 1. Top (a), bottom (b) and cross-section schematic views (c) of the proposed piezoelectric MEMS transducer.

standing-wave node thus forming a regular pattern with a gap of half the acoustic wavelength [20].

III. MEMS DESCRIPTION

More generally than the scope of the present study, the employed piezoelectric MEMS transducer has been designed as a versatile platform that can be exploited to investigate different applications [27], [28]. The PiezoMUMPs process by MEMSCAP [29] has been used for fabrication.

Figure 2a shows the bottom view of the 9 mm × 9 mm device taken from the graphic design system (GDS) file. The 6 mm × 6 mm diaphragm is a stack of a highly doped silicon layer (Si) and an aluminum nitride (AlN) piezoelectric layer. The MEMS design has been accomplished by considering the acoustic-fluidic coupling between water and the composite Si-AlN diaphragm. Specifically, the condition in which the wavelength of the A0 flexural mode in the diaphragm and the wavelength of the longitudinal waves in water are equal has been estimated taking into account the frequency-to-wavelength relationships described by [30] and [31]:

$$f_{A0} = \frac{2\pi t}{\lambda^2}\sqrt{\frac{E}{12(1-\eta^2)\rho}}\frac{1}{\sqrt{\frac{\pi^2 t^2}{3\lambda^2}+1}}, \tag{1}$$

and

$$f_w = \frac{c_w}{\lambda}, \tag{2}$$

where $E = 167$ GPa, $\eta = 0.268$, $\rho = 2373$ kg/m^3 and $t = 10.5$ μm are the overall, i.e. effective, Young's modulus, Poisson's ratio, mass density and thickness of the composite Si-AlN diaphragm, respectively, while $c_w = 1460$ m/s is the sound speed in water. By employing (1), (2) and considering tolerances in layer thicknesses due to the manufacturing process, λ is estimated as 112 ± 11 μm which corresponds to an excitation frequency range of $f_{exc} = 13 \pm 1.4$ MHz to match f_{A0}. Considering the nominal case, cells dispersed in the liquid are expected to be trapped and aligned along a regularly spaced pattern with a gap of $\lambda/2 = 56$ μm.

For the actuation of the AlN layer, eight IDTs are made available, each composed of two interleaved comb-shaped electrodes of twenty equally spaced fingers. As visible in Figure 2b, to ensure the generation of standing acoustic waves with wavelength $\lambda = 112$ μm, the pitch p has been set equal to λ and the distance d between two opposite IDTs has been set to 34λ [32], while the finger width w is 28 μm. The IDT rectangular pads are made by a metal stack of 20 nm of chrome (Cr) and 1 μm of aluminum (Al). The four squared metal pads at the corners electrically connect the doped silicon layer of the diaphragm. Figure 2c shows the X-X' cross section view where the silicon dioxide (SiO_2) layer and the silicon (Si) substrate layer are visible with a thickness of 1 ± 0.05 μm and 400 ± 5 μm, respectively. The thicknesses of the AlN and doped silicon diaphragm layers are 0.5 μm and 10 ± 1 μm, respectively. Top- and bottom-view images of the fabricated device are shown in Figure 3a,b, respectively. The cavity employed to confine the cells dispersed in liquid can be noticed.

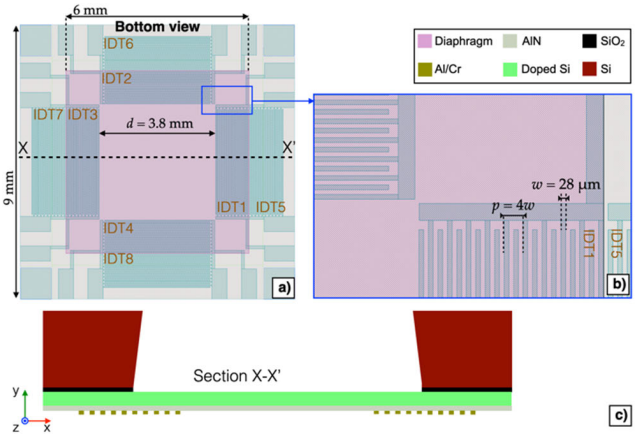

FIGURE 2. Bottom-view image of the designed piezoelectric MEMS (a), enlarged view of the IDTs (b) taken from the graphic design system (GDS) file, and cross-section view at X-X' (c).

IV. FINITE ELEMENT ANALYSIS

A 2D finite element model in COMSOL Multiphysics® has been developed to investigate the electro-mechanical behaviour and working principle of the piezoelectric MEMS described in Section II.

The cross-section of the simulated device and the structural layers that have been included in the 2D model are shown in Figure 4a,b, respectively. The metal layer has been considered as made by Al only, since its thickness is 50 times higher than the Cr thickness. The metal pads of the doped silicon layer have not been included in the model. <100> Si has been adopted for both the substrate and the silicon layer, while SiO_2 has been used as the oxide layer material.

For the AlN layer the piezoelectric coefficients have been specified as $d_{31} = -2.78$ pC/N and $d_{33} = 6.5$ pC/N [33].

The piezoelectric multiphysics has been used to simulate the piezoelectric effect, combining the physics of solid mechanics and electrostatics.

Strain-charge constitutive relations and dielectric losses have been specified considering the AlN material properties, and a charge conservation boundary condition has been

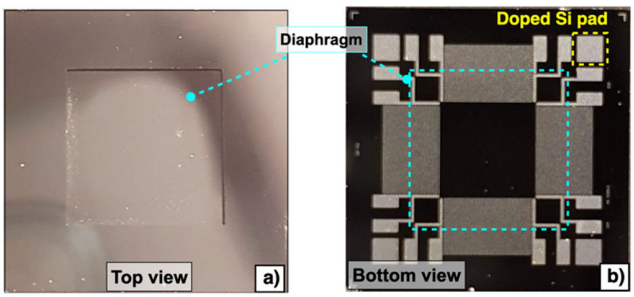

FIGURE 3. Top (a) and bottom (b) images of the fabricated piezoelectric MEMS.

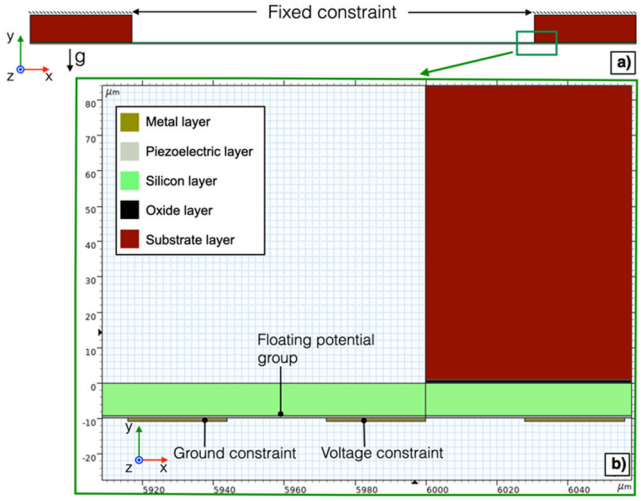

FIGURE 4. 2D model view of the proposed piezoelectric MEMS transducer (a). Enlarged image of the layers considered in the simulation model (b).

applied to the AlN layer in the electrostatics physics. As a simplifying assumption, an isotropic damping constraint has been applied to the whole structure with a loss factor of 0.004. Electrical domain conditions have been set to the IDTs fingers located on the diaphragm by alternating voltage and ground constraints. To simulate the high doping concentration, a floating potential group has been applied to the surface of the silicon layer in contact with AlN, thus modelling a conductive electrode. The mesh has been carefully adjusted to obtain a convergent solution while containing the computational workload as shown in Figure 5a. Horizontally, a mapped mesh distribution size of 1 μm has been adopted, as visible in Figure 5b. A mapped distribution mesh size of 0.5 μm, 0.1 μm, 1 μm, 1 μm and 200 μm has been set for the thicknesses of metal, piezoelectric, doped silicon, oxide, and substrate silicon layers, respectively.

A frequency domain study has been performed to evaluate the electrical admittance $Y(f)$ of a single IDT seen as a one-port element, defined as the ratio between the current collected at the IDT fingers $i_c(t)$ and the applied sinusoidal excitation voltage $v_{exc}(t)$, with rms amplitude A_{exc} set to 1 V,

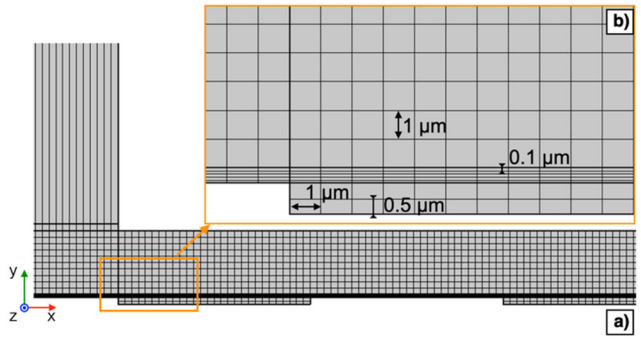

FIGURE 5. Mesh domain of the proposed piezoelectric MEMS transducer (a). Enlarged image of the mesh for metal, piezoelectric and silicon layers (b).

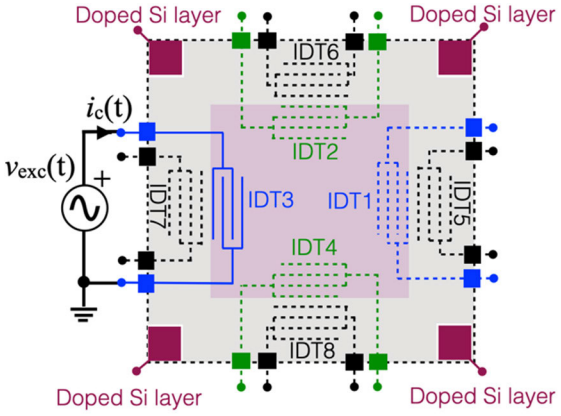

FIGURE 6. Schematic view of the proposed piezoelectric MEMS transducer configured for the simulation of the electrical admittance of IDT3.

both converted in the frequency domain. Specifically, the IDT3 located on the inner side of the diaphragm has been analysed while leaving all other IDTs floating, as shown in Figure 6. In accordance with the frequency range derived in Section III, the excitation frequency f_{exc} has been varied from 10 to 15 MHz with a step size of 12.5 kHz. Figure 7 plots the obtained real and imaginary parts of the electrical admittance $Y(f)$ of IDT3 as a function of the excitation frequency f_{exc}.

The obtained admittance pattern is mainly determined by the IDT3 location on the diaphragm. Acoustic waves are generated and propagated towards both the proximate and far boundaries of the diaphragm which behave as wave reflectors. Since IDT3 is not located in the centre of the diaphragm, the distance travelled by the acoustic waves to reach the reflectors differs [34], [35], [36]. This leads to the generation

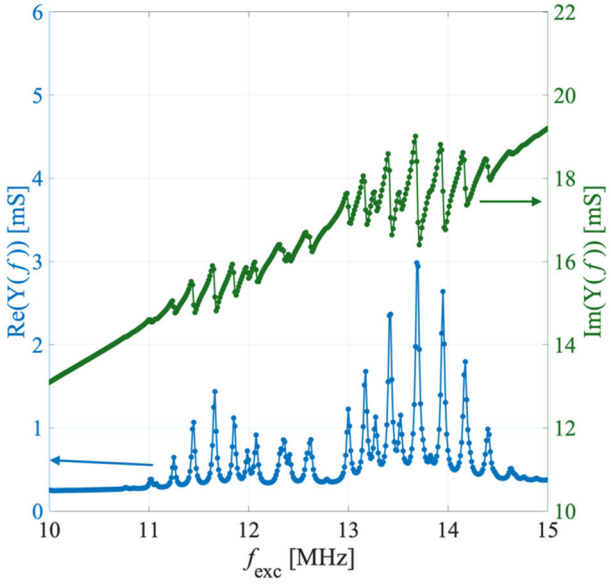

FIGURE 7. Simulated real (blue, left y-axis) and imaginary (green, right y-axis) parts of the admittance $Y(f)$ of a single IDT as a function of the excitation frequency f_{exc}.

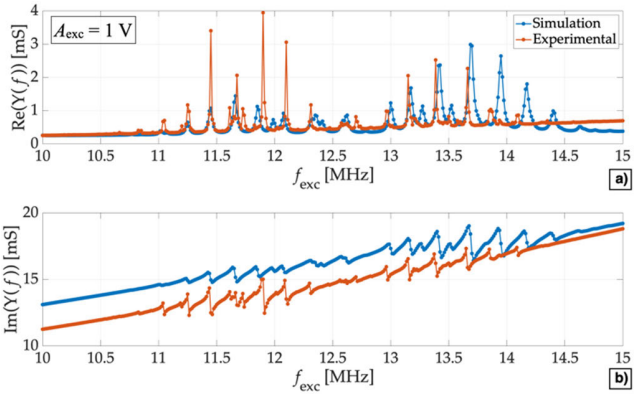

FIGURE 8. Comparison between simulated (blue) and measured (orange) real (a) and imaginary (b) part of the admittance $Y(f)$ of a single IDT as a function of the excitation frequency f_{exc}.

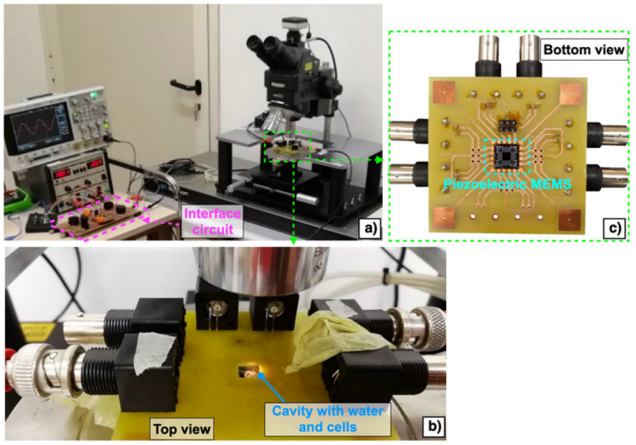

FIGURE 10. Experimental setup employed to align cells in water (a). Top (b) and bottom (c) views of the dedicated PCB hosting the piezoelectric MEMS transducer.

of distinct sets of peaks in the real part of $Y(f)$ between 10.8 and 12.8 MHz and between 12.8 and 14.8 MHz. The obtained peaks are consistent with the estimated frequency range $f_{exc} = 13 \pm 1.4$ MHz obtained from the acoustic-fluidic coupling for an unbounded plate described in Section II.

V. EXPERIMENTAL RESULTS

To validate the simulated results described in Section V, the electrical admittance versus frequency of the single IDT3 has been experimentally measured by means of a HP4194A analyzer while the other IDTs have been left floating. A sinusoidal excitation with rms amplitude A_{exc} of 1 V has been used with the frequency f_{exc} swept between 10 and 15 MHz with a step size of 12.5 kHz. The measured real and imaginary parts of the admittance $Y(f)$ are plotted in Figure 8a,b and compared with the corresponding results obtained from simulations.

The agreement between simulated and experimental results within the explored frequency range is remarkable. The residual discrepancies can be possibly due to the fabrication process tolerances and the simplifying assumptions adopted for the 2D model described in Section IV. The cell alignment with 1D acoustic field pattern generated through standing FPWs has been experimentally verified at room temperature by exciting both IDT1 and IDT3, which are located on the inner opposite sides of the diaphragm as shown in the

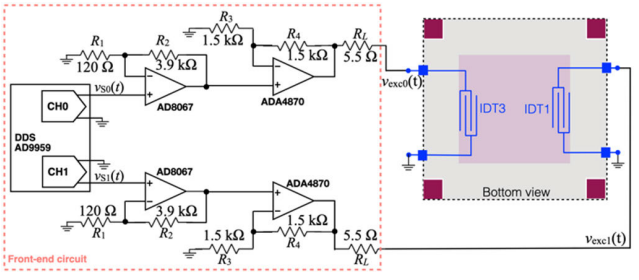

FIGURE 9. Block diagram of the circuit employed to excite two IDTs for generating 1D acoustic field pattern.

block diagram of the electronics of Figure 9. The sinusoidal excitation voltage $v_{exc}(t)$ has been generated by employing a tailored front-end circuit based on the direct digital synthesizer (DDS) (Analog Devices AD9959) which embeds four independent output channels. The interface circuit has been devised as a general-purpose system for the excitation of either 1D or 2D acoustic field patterns. In this work, only two channels of the DDS have been employed to generate a 1D acoustic pattern, at the same time exploiting a fine frequency tuning to generate two sinusoidal voltages $v_{s0}(t)$ and $v_{s1}(t)$ with same peak amplitude of 250 mV and zero relative phase shift. The signals $v_{s0}(t)$ and $v_{s1}(t)$ are amplified with a nominal gain of 40 at 15 MHz by wide-bandwidth noninverting amplifiers (Analog Devices AD8067 and ADA4870) and fed to the two IDTs to properly drive the equivalent capacitive load at up to 15 MHz. The experimental setup developed to perform the alignment of cells is shown in Figure 10a. The MEMS has been mounted on a dedicated printed circuit board (PCB) as shown in the top and bottom views of Figure 10b,c, respectively. The MEMS cavity has been filled with inactive fibroblast cells with an approximate diameter d_p of 15 μm dispersed in demineralized water with a concentration in the order of 10^5 cells/ml as shown in the image of Figure 11a captured with a Motic PSM-1000 microscope (Motic: Wetzlar, Germany). Liquid and cells have been placed in the cavity by means of a syringe kept at a fixed distance from the diaphragm to avoid damage.

The excitation voltages $v_{exc0}(t)$ and $v_{exc1}(t)$ both with peak amplitude of 10 V have been applied to IDT1 and IDT3, respectively. The same excitation frequency f_{exc} of both signals has been finely tuned until cell alignment was clearly observed. This approach allows to accurately adjust to the target condition. As shown in Figure 11b, ordered alignment has been reached at f_{exc} =12.5 MHz, in agreement with the expected range predicted in Section III. From the enlarged image of Figure 11c the nominal spacing between two adjacent lines of cells in the alignment pattern can be estimated as 56 μm corresponding to half the acoustic wavelength,

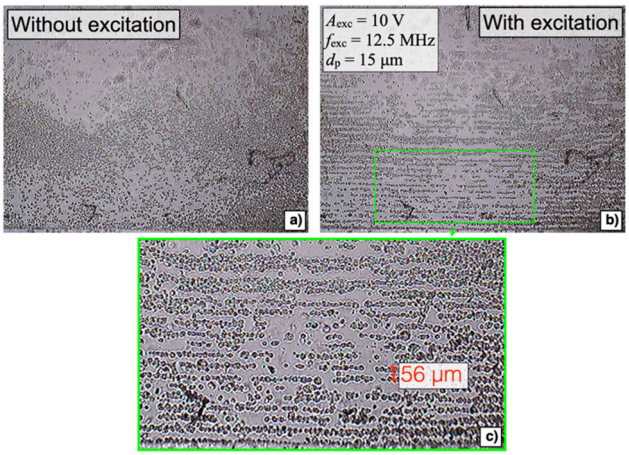

FIGURE 11. Images of fibroblast cells dispersed in demineralized water placed in the MEMS cavity without (a) and with (b) voltage excitation applied. Enlarged view of the cells aligned at a nominal spacing of 56 μm (c).

in accordance with theoretical expectations. The obtained experimental results confirm that the proposed piezoelectric MEMS transducer can be successfully employed to align cells dispersed in water by means of flexural plate waves.

VI. CONCLUSION

This work has presented a piezoelectric MEMS transducer to generate a 1D acoustic field pattern for cell alignment in aqueous solution by means of standing flexural plate waves (FPWs). The 9 mm × 9 mm MEMS includes a squared cavity formed by a 6 mm × 6 mm composite diaphragm of doped silicon (Si) and aluminum nitride (AlN) layers to steer cells dispersed in water. By properly setting the metal interdigital transducers (IDTs) pitch over the AlN film, the A0 flexural mode in the composite diaphragm and the longitudinal waves in water can be excited at the same frequency. Therefore, cell alignment in water can be achieved by vibrating the diaphragm. The expected excitation frequency range at around 12.5 MHz has been confirmed by analysing the electrical impedance of a single IDT through a 2D finite element modelling in COMSOL Multiphysics® and by comparing the simulation and experimental results. A tailored front-end electronic circuit, based on a two-channel direct digital synthesizer (DDS), has been developed to generate two inusoidal excitation signals with peak amplitude of 10 V, zero relative phase shift at up to 15 MHz. Inactive fibroblast cells with an approximate diameter of 15 μm dispersed in demineralized water with a concentration in the order of 10^5 cells/ml have been placed in the MEMS cavity. The generated excitation signals have been fed to two IDTs located at the opposite inner sides of the diaphragm allowing to successfully achieve cell alignment at the excitation frequency of 12.5 MHz. The spacing between two adjacent cell lines in the alignment pattern has been optically estimated as 56 μm corresponding to half the acoustic wavelength. This validates the proposed MEMS transducer as a microdevice to generate a 1D acoustic field pattern in aqueous solution for cell alignment. Future activities will include the exploitation of 2D acoustic field pattern by driving four IDTs and the embodiment of the MEMS into a dedicated lab-on-chip system to further expand the application possibilities.

ACKNOWLEDGMENT

The contribution of Maurizio Antonini and Mattia Minelli to the laboratory activity is acknowledged.

REFERENCES

[1] C. D. Devillard and C. A. Marquette, "Vascular tissue engineering: Challenges and requirements for an ideal large scale blood vessel," *Frontiers Bioeng. Biotechnol.*, vol. 9, Oct. 2021, Art. no. 721843, doi: 10.3389/fbioe.2021.721843.

[2] T. Koorman, K. A. Jansen, A. Khalil, P. D. Haughton, D. Visser, M. A. K. Rätze, W. E. Haakma, G. Sakalauskaitè, P. J. van Diest, J. de Rooij, and P. W. B. Derksen, "Spatial collagen stiffening promotes collective breast cancer cell invasion by reinforcing extracellular matrix alignment," *Oncogene*, vol. 41, no. 17, pp. 2458–2469, Apr. 2022, doi: 10.1038/s41388-022-02258-1.

[3] J. Du, J. Liu, S. Yao, H. Mao, J. Peng, X. Sun, Z. Cao, Y. Yang, B. Xiao, Y. Wang, P. Tang, and X. Wang, "Prompt peripheral nerve regeneration induced by a hierarchically aligned fibrin nanofiber hydrogel," *Acta Biomaterialia*, vol. 55, pp. 296–309, Jun. 2017, doi: 10.1016/j.actbio.2017.04.010.

[4] L. Zhu, S. Jia, T. Liu, L. Yan, D. Huang, Z. Wang, S. Chen, Z. Zhang, W. Zeng, Y. Zhang, H. Yang, and D. Hao, "Aligned PCL fiber conduits immobilized with nerve growth factor gradients enhance and direct sciatic nerve regeneration," *Adv. Funct. Mater.*, vol. 30, no. 39, Sep. 2020, Art. no. 2002610, doi: 10.1002/adfm.202002610.

[5] F. J. O'Brein, "Biomaterials & scaffolds for tissue engineering," *Mater. Today*, vol. 14, pp. 88–95, Mar. 2011, doi: 10.1016/S1369-7021(11)70058-X.

[6] K. J. Morton, K. Loutherback, D. W. Inglis, O. K. Tsui, J. C. Sturm, S. Y. Chou, and R. H. Austin, "Hydrodynamic metamaterials: Microfabricated arrays to steer, refract, and focus streams of biomaterials," *Proc. Nat. Acad. Sci. USA*, vol. 105, no. 21, pp. 7434–7438, May 2008, doi: 10.1073/pnas.0712398105.

[7] I. M. Basurto, S. A. Muhammad, G. M. Gardner, G. J. Christ, and S. R. Caliari, "Controlling scaffold conductivity and pore size to direct myogenic cell alignment and differentiation," *J. Biomed. Mater. Res. A*, vol. 110, no. 10, pp. 1681–1694, Oct. 2022, doi: 10.1002/jbm.a.37418.

[8] D. G. Grier, "A revolution in optical manipulation," *Nature*, vol. 424, no. 6950, pp. 810–816, Aug. 2003, doi: 10.1038/nature01935.

[9] P. Y. Chiou, A. T. Ohta, and M. C. Wu, "Massively parallel manipulation of single cells and microparticles using optical images," *Nature*, vol. 436, no. 7049, pp. 370–372, Jul. 2005, doi: 10.1038/nature03831.

[10] B. B. Yellen, O. Hovorka, and G. Friedman, "Arranging matter by magnetic nanoparticle assemblers," *Proc. Nat. Acad. Sci. USA*, vol. 102, no. 25, pp. 8860–8864, Jun. 2005, doi: 10.1073/pnas.0500409102.

[11] C. Y. Fan, Y.-C. Tung, S. Takayama, E. Meyhöfer, and K. Kurabayashi, "Electrically programmable surfaces for configurable patterning of cells," *Adv. Mater.*, vol. 20, no. 8, pp. 1418–1423, Apr. 2008, doi: 10.1002/adma.200702191.

[12] C. Y. Fan, K. Kurabayashi, and E. Meyhöfer, "Protein pattern assembly by active control of a triblock copolymer monolayer," *Nano Lett.*, vol. 6, no. 12, pp. 2763–2767, Dec. 2006, doi: 10.1021/nl061780y.

[13] V. Perrotti, A. Piattelli, A. Quaranta, G. Gómez-Moreno, and G. Iezzi, "1-biocompatibility of dental biomaterials," in *Biocompatibility of Dental Biomaterials*, R. Shelton, Ed. Sawston, U.K.: Woodhead, 2017, pp. 1–7, doi: 10.1016/B978-0-08-100884-3.00001-1.

[14] M. A. Burguillos, C. Magnusson, M. Nordin, A. Lenshof, P. Augustsson, M. J. Hansson, E. Elmér, H. Lilja, P. Brundin, T. Laurell, and T. Deierborg, "Microchannel acoustophoresis does not impact survival or function of microglia, leukocytes or tumor cells," *PLoS ONE*, vol. 8, no. 5, May 2013, Art. no. e64233, doi: 10.1371/journal.pone.0064233.

[15] T. Zheng, C. Wang, C. Xu, Q. Hu, and S. Wei, "Patterning microparticles into a two-dimensional pattern using one column standing surface acoustic waves," *Sens. Actuators A, Phys.*, vol. 284, pp. 168–171, Dec. 2018, doi: 10.1016/j.sna.2018.10.001.

[16] A. L. Bernassau, P. Glynne-Jones, F. Gesellchen, M. Riehle, M. Hill, and D. R. S. Cumming, "Controlling acoustic streaming in an ultrasonic heptagonal tweezers with application to cell manipulation," *Ultrasonics*, vol. 54, no. 1, pp. 268–274, Jan. 2014, doi: 10.1016/j.ultras.2013.04.019.

[17] T. Laurell, F. Petersson, and A. Nilsson, "Chip integrated strategies for acoustic separation and manipulation of cells and particles," *Chem. Soc. Rev.*, vol. 36, no. 3, pp. 492–506, 2007, doi: 10.1039/b601326k.

[18] M. Serzanti, M. Bau, M. Demori, S. Calamaio, M. Cominelli, P. L. Poliani, P. Dell'Era, M. Ferrari, and V. Ferrari, "Arrangement of live human cells through acoustic waves generated by piezoelectric actuators for tissue engineering applications," *Appl. Sci.*, vol. 10, no. 10, p. 3477, May 2020, doi: 10.3390/app10103477.

[19] P. Reichert, D. Deshmukh, L. Lebovitz, and J. Dual, "Thin film piezoelectrics for bulk acoustic wave (BAW) acoustophoresis," *Lab Chip*, vol. 18, no. 23, pp. 3655–3667, 2018, doi: 10.1039/c8lc00833g.

[20] F. Guo, Z. Mao, Y. Chen, Z. Xie, J. P. Lata, P. Li, L. Ren, J. Liu, J. Yang, M. Dao, S. Suresh, and T. J. Huang, "Three-dimensional manipulation of single cells using surface acoustic waves," *Proc. Nat. Acad. Sci. USA*, vol. 113, no. 6, pp. 1522–1527, Feb. 2016, doi: 10.1073/pnas.1524813113.

[21] C. Walk, M. Wiemann, M. Görtz, J. Weidenmüller, A. Jupe, and K. A. Seidl, "A piezoelectric flexural plate wave (FPW) bio-MEMS sensor with improved molecular mass detection for point-of-care diagnostics," *Current Directions Biomed. Eng.*, vol. 5, no. 1, pp. 265–268, 2019, doi: 10.1515/cdbme-2019-0067.

[22] V. Ferrari and R. Lucklum, "Overview of acoustic-wave microsensors," in *Piezoelectric Transducers and Applications*, A. A. Vives, Eds. Berlin, Germany: Springer, 2008.

[23] A. Nastro, M. Bau, M. Ferrari, L. Rufer, S. Basrour, and V. Ferrari, "Flexural plate wave piezoelectric MEMS transducer for cell alignment in aqueous solution," in *Proceedings of SIE* (Lecture Notes in Electrical Engineering), vol. 1005, G. Cocorullo, F. Crupi, and E. Limiti, Eds. Cham, Switzerland: Springer, 2022, doi: 10.1007/978-3-031-26066-7_19.

[24] D. J. Collins, B. Morahan, J. Garcia-Bustos, C. Doerig, M. Plebanski, and A. Neild, "Two-dimensional single-cell patterning with one cell per well driven by surface acoustic waves," *Nature Commun.*, vol. 6, no. 1, p. 8686, Nov. 2015, doi: 10.1038/ncomms9686.

[25] X. Ding, J. Shi, S.-C.-S. Lin, S. Yazdi, B. Kiraly, and T. J. Huang, "Tunable patterning of microparticles and cells using standing surface acoustic waves," *Lab Chip*, vol. 12, no. 14, p. 2491, 2012, doi: 10.1039/c2lc21021e.

[26] X. Ding, S.-C.-S. Lin, B. Kiraly, H. Yue, S. Li, I.-K. Chiang, J. Shi, S. J. Benkovic, and T. J. Huang, "On-chip manipulation of single microparticles, cells, and organisms using surface acoustic waves," *Proc. Nat. Acad. Sci. USA*, vol. 109, no. 28, pp. 11105–11109, Jul. 2012, doi: 10.1073/pnas.1209288109.

[27] A. Nastro, M. Baù, M. Ferrari, and V. Ferrari, "Piezoelectric MEMS for sensors, actuators and energy harvesting," in *Sensors and Microsystems*, vol. 918. Cham, Switzerland: Springer, 2023, doi: 10.1007/978-3-031-08136-1_41.

[28] A. Nastro, L. Rufer, M. Ferrari, S. Basrour, and V. Ferrari, "Piezoelectric micromachined acoustic transducer with electrically-tunable resonant frequency," in *Proc. 20th Int. Conf. Solid-State Sensors, Actuat. Microsystems Eurosensors*, Jun. 2019, pp. 1905–1908, doi: 10.1109/TRANSDUCERS.2019.8808488.

[29] A. Cowen, G. Hames, K. Glukh, and B. Hardy, *PiezoMUMPs Design Handbook*, 3rd ed. Durham, NC, USA: MEMSCAP, 2014.

[30] M. Demori, M. Baù, M. Ferrari, S. Basrour, L. Rufer, and V. Ferrari, "MEMS device with piezoelectric actuators for driving mechanical vortexes in aqueous solution drop," in *Proc. 20th Int. Conf. Solid-State Sensors, Actuat. Microsystems Eurosensors*, Jun. 2019, pp. 2318–2321, doi: 10.1109/TRANSDUCERS.2019.8808791.

[31] Y. Liu, Y. Li, A. M. El-Hady, C. Zhao, J. F. Du, Y. Liu, and Y. Q. Fu, "Flexible and bendable acoustofluidics based on ZnO film coated aluminium foil," *Sens. Actuators B, Chem.*, vol. 221, pp. 230–235, Dec. 2015, doi: 10.1016/j.snb.2015.06.083.

[32] J. Qian, J. Ren, W. Huang, R. H. W. Lam, and J. E.-Y. Lee, "Acoustically driven manipulation of microparticles and cells on a detachable surface micromachined silicon chip," *IEEE Sensors J.*, vol. 21, no. 10, pp. 11999–12008, May 2021, doi: 10.1109/JSEN.2021.3065694.

[33] A. Nastro, M. Ferrari, L. Rufer, S. Basrour, and V. Ferrari, "Piezoelectric MEMS acoustic transducer with electrically-tunable resonant frequency," *Micromachines*, vol. 13, no. 1, p. 96, Jan. 2022, doi: 10.3390/mi13010096.

[34] D. W. Branch, K. E. Wojciechowski, and R. H. Olsson, "Elucidating the origin of spurious modes in aluminum nitride microresonators using a 2-D finite-element model," *IEEE Trans. Ultrason., Ferroelectr., Freq. Control*, vol. 61, no. 5, pp. 729–738, May 2014, doi: 10.1109/TUFFC.2014.2965.

[35] M. S. Weinberg, B. T. Cunningham, and C. W. Clapp, "Modeling flexural plate wave devices," *J. Microelectromech. Syst.*, vol. 9, no. 3, pp. 370–379, Sep. 2000, doi: 10.1109/84.870063.

[36] G. Quentin, A. Derem, and B. Poirée, "Group velocity and acoustical resonances," *J. de Phys.*, vol. 50, no. 14, pp. 1943–1952, 1989, doi: 10.1051/jphys:0198900500140194300.

ALESSANDRO NASTRO (Member, IEEE) was born in Romano di Lombardia, Italy, in 1991. He received the master's degree (cum laude) in electronics engineering and the Europaeus Ph.D. degree in information engineering from the University of Brescia, in 2016 and 2020, respectively. Since 2019, he has been a Research Fellow of electronics with the Department of Information Engineering, University of Brescia, where he has been an Assistant Professor, since May 2022. He has co/authored more than 20 publications in international peer-reviewed journals and international and national conference proceedings. His research interests include the development of electronic techniques and circuits coupled to MEMS for static and dynamic micromechanical sensing and actuation.

MARCO BAÙ (Member, IEEE) was born in Castiglione delle Stiviere, Italy, in 1981. He received the Laurea degree (cum laude) in electronic engineering and the Research Ph.D. degree in electronic instrumentation from the University of Brescia, in 2005 and 2009, respectively. From 2009 to September 2018, he was a Research Assistant of electronics with the Department of Information Engineering, University of Brescia, where he has been an Assistant Professor, since October 2018. His research interests include the investigation of techniques for the contactless interrogation of resonant and capacitive sensors for autonomous electronics devices, the design of MEMS sensors and the related front-end electronic circuits, and the investigation of principles and techniques for energy harvesting from vibrations adopting linear and non-linear conversion techniques.

MARCO FERRARI (Member, IEEE) was born in Brescia, Italy, in 1974. He received the Laurea degree in electronics engineering and the Research Ph.D. degree in electronic instrumentation from the University of Brescia, in 2002 and 2006, respectively. He was an Assistant Professor (2007–2015) and an Associate Professor (2015–2020) with the Department of Information Engineering, University of Brescia, where he has been a Full Professor of electronics, since 2020. He is currently an Associate Member with the Italian National Research Council (CNR), National Institute of Nuclear Physics (INFN). He has co/authored more than 100 publications in international peer-reviewed journals and international conference proceedings and a patent with industrial exploitation. His research interests include the energy conversion via the piezoelectric and thermoelectric effect for powering autonomous microsystems, sensors for physical and chemical quantities, signal-conditioning electronics, oscillators and frequency-output interface circuits, resonant microsensors, and MEMS.

LIBOR RUFER (Senior Member, IEEE) received the engineering and Ph.D. degrees from Czech Technical University in Prague, Prague. Until 1993, he was with the Faculty of Electrical Engineering, Czech Technical University in Prague. Since 1994, he has been an Associate Professor, and later a Senior Scientist with Université Grenoble Alpes, France. In 1998, he joined the Microsystems Group, TIMA Laboratory. Since 2021, he has been with Advanced Design and Technology for MEMS (ADT MEMS). He is the author of more than 150 papers in refereed international journals and conferences. He participated in number of French and European projects. His research interests include MEMS-based sensors and actuators, electroacoustic and electromechanical transducers and their applications in acoustics, ultrasonics, and energy harvesting. He is a committee member of competitive international conferences and a reviewer of number of prestigious journals and conferences in the field of MEMS and acoustics.

SKANDAR BASROUR (Member, IEEE) received the degree from École Normale Supérieure de Tunis, Tunis, Tunisia, in 1986, and the Ph.D. degree in microelectronics from Université Joseph Fourier, Grenoble, France, in 1990. From 1992 to 2001, he was an Assistant Professor of electronics and microsystems with Université de Franche-Comté, Besançon, France. He contributed to the development and the improvement of the X-ray and UV LIGA microfabrication techniques. Since 2001, he has been a Full Professor of electronics and microsystems with the Polytech School of Engineering, Université Grenoble Alpes, Grenoble. He was the Leader of the TIMA Laboratory, Micro and Nano Systems Group, for 12 years. Since 2013, he has been the Co-Leader of the CDSI Group, TIMA Laboratory, Grenoble. Since 2015, he has been the Deputy Director of the TIMA Laboratory. His research interests include design, fabrication, and characterization of high-Q microresonator and nanoresonator as a time reference. In recent years, he propelled the design of new micropower generators based on piezoelectric thin films (PiezoMEMS). More recently, he started working on acoustic devices, such as microphones for aeroacoustics metrology and tactile devices using ultrasound waves for haptic rendering.

VITTORIO FERRARI (Senior Member, IEEE) received the Laurea degree (cum laude) in physics from the University of Milan, in 1988, and the Ph.D. degree in electronic instrumentation from the University of Brescia, Italy, in 1993. He has been a Full Professor of electronics with the University of Brescia, since 2006. From 2016 to 2022, he was the Rectors's delegate for research quality management and postgraduate studies with the University of Brescia. He is currently an Associate Member with the Italian National Research Council (CNR), National Institute of Nuclear Physics (INFN). He has authored and coauthored more than 250 publications in international peer-reviewed journals and conference proceedings, invited presentations, book chapters, and seven patents. He and his group are active in research projects, with both academic and industrial participation, on piezoelectric transducers and resonant microsensors, energy harvesting for autonomous sensors, MEMS and microsystems, sensors with contactless interrogation, electronic interfaces for sensor signals, sensing systems for fluidics, and wearable devices. He serves in international panels, conference committees, including IEEE UFFC-IUS Group 5, and boards in the field of sensors and electronic instrumentation. He was the Program Chair of the Eurosensors Conference 2014.

Open Access funding provided by 'Università degli Studi di Brescia' within the CRUI CARE Agreement